Journal of Applied Electrochemistry (2020) 50:311–319
https://doi.org/10.1007/s10800-019-01391-2

RESEARCH ARTICLE

Electrochemical determination of dopamine using a conductive polypyrrole/carbon-coated mesoporous silica composite electrode

Yu-Che Liu[1] · Wei-Fang Hsu[1] · Tzong-Ming Wu[1]

Received: 14 August 2019 / Accepted: 16 December 2019 / Published online: 3 January 2020

Abstract

Mesoporous silica (SiO_2) nanoparticles were prepared using the cationic surfactant cetyltrimethylammonium bromide as a soft template in a basic medium. The particles were coated with a carbon layer through a facile hydrothermal process. The carbon-coated mesoporous SiO_2 (C#SiO_2) nanoparticles were used as core for the in situ chemical-oxidative polymerization of conductive polypyrrole (PPy). The structure and morphology of the PPy/C#SiO_2 nanocomposites were analyzed by transmission electron microscopy, wide-angle X-ray diffraction, and Fourier transform infrared spectroscopy. A glassy carbon electrode was modified with the PPy/C#SiO_2 nanocomposites. The performance of the modified electrode for the dopamine (DA) detection was examined by cyclic voltammetry, electrochemical impedance spectroscopy, and differential pulse voltammetry. The modified PPy/C#SiO_2 glassy carbon electrode exhibit large peak currents for the DA oxidation reaction, suggesting the electrochemical performance of the nanocomposites is enhanced. The impedance evaluation of the fabricated PPy/C#SiO_2 nanocomposites reveals a very small charge-transfer resistance. Additionally, the nanocomposites showed a linear response for DA detection in the concentration range of 1×10^{-6} to 2×10^{-4} M with a detection limit of 7.6×10^{-7} M ($S/N=3$). Moreover, DA detection was successful in the presence of uric acid and L-ascorbic acid. Due to their outstanding electrochemical performance, the PPy/C#SiO_2 nanocomposites may be considered for the DA detection devices.

✉ Tzong-Ming Wu
tmwu@dragon.nchu.edu.tw

[1] Department of Materials Science and Engineering, National Chung Hsing University, 250 Kuo Kuang Road, Taichung 402, Taiwan

Graphic abstract

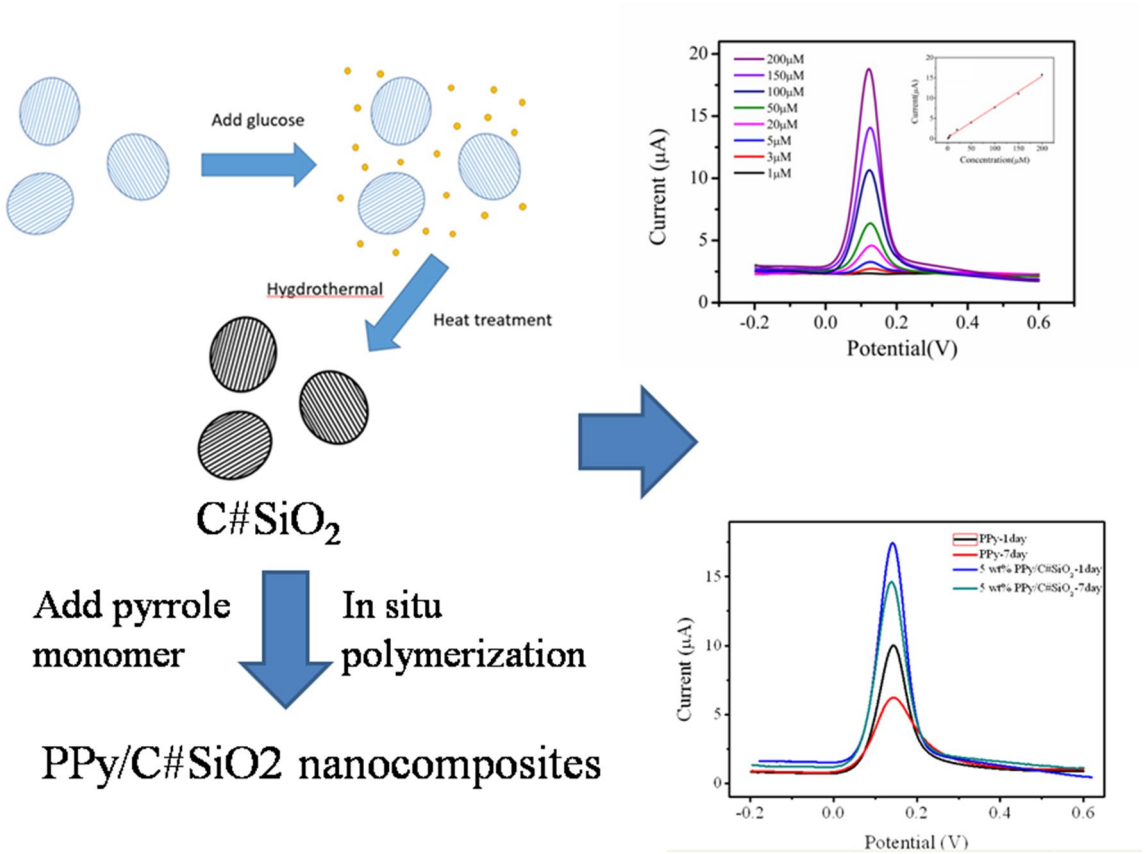

Keywords Polypyrrole · Mesoporous silica nanoparticles · Nanocomposite · Dopamine · Biosensor

1 Introduction

Catecholamines are important biogenic neurotransmitters, crucial for communication between neurons. Dopamine (DA), one of the most relevant among these neurotransmitters, serves an important role as it is extensively distributed in the mammalian brain [1, 2]. Abnormal DA concentrations are associated with Alzheimer's and Parkinson's disease, and schizophrenia [3]. Therefore, the development of an accurate, quick, and simple analytical method for DA detection is of great importance. Several approaches have been proposed for DA detection and determination [4, 5]. In particular, the electrochemical method is widely used because it is simple, fast, and accurate. However, DA detection using bare electrodes in blood and urine samples is difficult due to the interference of coexisting species, for example, ascorbic (AA) and uric (UA) acid [6]. Hence, various materials, such as carbon nanotubes [7], graphene [8], graphene quantum dots [9], gold nanoparticles [10], and Cu_2O/graphene [11] have been used to obtain the modified working electrodes. For instance, Zhang et al. [7] prepared a modified glassy carbon electrode (GCE) with lanthanum–multi-walled carbon nanotubes (MWCNT) nanocomposites for simple and sensitive detection of AA, DA, UA, and nitrite. Raj et al. [10] obtained a GCE modified with gold nanoparticles with excellent DA detection. Zhang et al. [11] reported the easy fabrication of Cu_2O/graphene nanocomposites via one-pot solvothermal synthesis. The nanocomposite was used to modify a GCE and a high-DA electrocatalytic activity was achieved.

Intrinsically conducting polymers have gained a lot of attention owing to their excellent electrical and physical properties [12, 13]. Due to its stability, ease of synthesis and high-electrical conductivity, polypyrrole (PPy) has been extensively investigated for different applications, i.e., sensors, solid electrodes for capacitors, and electronic devices [14–16].

Ghanbari et al. [15] found that the metal oxide nanoparticles have an outstanding electrochemical performance under oxidative and acidic circumstances. They also have

a significant effect on the electrochemical properties of materials. Recently, metal oxides, such as silica (SiO_2), TiO_2, NiO, and SnO_2, have been used to improve polymeric materials because of their tremendous mechanical and thermal properties [17–19].

PPy composites with carbon materials or metal oxides have been used for highly selective sensors in DA detection [20–22]. Sensors with various surface morphologies exhibit a high surface to volume ratio, which can enhance their electrocatalytic activity [23]. Thus, mesoporous SiO_2 nanoparticles with different surface morphologies have been widely used in sensors, for adsorption processes, in medical applications and for nanotechnology [24–26].

In this study, a new approach contained both carbon material and metal oxide in one material was prepared using the coating of carbon material on the surface of metal oxide. The mesoporous metal oxide SiO_2 nanoparticles were prepared using the cationic surfactant cetyltrimethylammonium bromide (CTAB) as a soft template in a basic medium. Then, the nanoparticles were coated with a carbon layer through a facile hydrothermal process in an aqueous glucose solution followed by calcination at 550 °C under nitrogen. The carbon-coated mesoporous SiO_2 nanoparticles (C#SiO_2) acted as a core for the preparation of conductive PPy/C#SiO_2 nanocomposites via in situ chemical-oxidative polymerization. The electrochemical properties of the composites were investigated. Then, using the PPy/C#SiO_2 nanocomposites, we developed an electrochemical biosensor for DA detection.

2 Experimental

2.1 Materials

L-ascorbic acid (AA), cetyltrimethylammonium bromide (CTAB), dopamine (DA), glucose, pyrrole monomer, tetraethoxysilane (TEOS), urea and uric acid (UA) were purchased from Aldrich-Sigma (Taipei, Taiwan). Ammonium peroxydisulfate (APS) was obtained from JT-Baker (Hsinchu Hsien, Taiwan). Pyrrole monomer was purified by distillation under reduced pressure. Other reagents were all analytical grade and used without further purification.

2.2 Preparation of carbon-coated mesoporous SiO_2 (C#SiO_2) nanoparticles

The mesoporous silica nanoparticles was prepared as follows: first, 3.5 mL of NaOH solution was added to 480 mL of distilled water (DI-water). The 1 g of cationic surfactant (CTAB) served as a soft template was mixed with the NaOH solution by stirring and heating at 80 °C. As the solution became homogeneous, 5 mL of tetraethoxysilane (TEOS) was slowly dropped into the mixture and continuously stirred for 2 h. The resulting product was filtered, washed several times with a mixture of DI-water and ethanol, dried for 24 h at 60 °C oven, and followed by a subsequent calcination in 550 °C in a nitrogen atmosphere. The carbon-coated mesoporous SiO_2 (C#SiO_2) nanoparticles were fabricated using the same approach to fabricate graphene quantum dots (GQDs) [27]. For the synthesis of C#SiO_2 nanoparticles with the core–shell structure, take 1 g of SiO_2 nanoparticles mixed with 10 mL of DI-water and sonicated for 1 h. Subsequently 1 g glucose powders were mixed with the SiO_2 solution and stirred for 24 h at 40 °C. The resultant solution was moved into autoclave for hydrothermal synthesis for 4 h at 200 °C. Finally, the resulting product was filtered, washed numerous times with a mixture of DI-water and ethanol, dried for 24 h at 60 °C oven, and followed by a subsequent calcination in 550 °C in a nitrogen atmosphere.

2.3 Preparation of PPy/C#SiO_2 nanocomposites

The PPy/C#SiO_2 nanocomposites were fabricated using in situ chemical-oxidative polymerization. Various weight ratio of C#SiO_2 were dispersed in 40 mL 1 M hydrochloric acid (HCl) solution by sonication. After 1 h, 0.01 mL pyrrole monomer was added into C#SiO_2 dispersion solution and stirred for 30 min. The 0.013 g of ammonium persulfate (APS) powders dissolved in 10 mL of 1 M HCl was dropped into the dispersion solution at 0 °C and keeps stirred for 3 h. After reaction, the resulting product were filtered, washed with a mixture of DI-water and methanol successively, and then dried for 24 h at 60 °C oven.

2.4 Material characterization

The Fourier transform infrared (FTIR) experiments were carried out on a Perkin–Elmer Spectrum One spectrometer (Waltham, Massachusetts, USA) from 400 to 4000 cm^{-1}. Raman spectra were performed with a TRIAX 550 Jobin–Yvon monochromator (HORIBA Scientific, United Kingdom) by a He–Ne laser operating at 633 nm as the excitation source. The presented spectrum is an average of at least three spectra measured at different regions over the entire sample range. The measurements of wide-angle X-ray diffraction (WAXD) were carried out on a X-ray diffractometer (Bruker D8, BRUKER AXS, Inc., Madison, Wisconsin, USA) equipped with a Ni-filtered Cu Kα radiation in the range of $2\theta = 5°–50°$ at 2°/min. The morphology was performed using a JEOL/JEM-2100F transmission electron microscopy (TEM) (JEOL Ltd., Tokyo, Japan). The specimens for TEM experiment were obtained using casting a drop of the specimen mixed in ethanol on a carbon-coated copper grid.

2.5 Electrochemical performance analyses

Electrochemical experiments were performed using a conventional three-electrode system, including an Ag/AgCl electrode as the reference electrode, a glassy carbon electrode (GCE) as the working electrode, and a platinum wire electrode as the counter electrode. The fabricated sample was ultrasonicated in DI-water, then coated on the surface of a lately polished GCE, and finally dried for 3 h at ambient atmosphere. Differential pulse voltammetry (DPV) measurements were performed using the scan rate of 5 mVS^{-1} at pH = 7 for the individual or simultaneous determination of AA, DA and UA.

3 Results and discussion

3.1 Chemical, structural, and morphological characterization

The wide-angle X-ray diffraction (WAXD) and transmission electron microscopy (TEM) were used to verify the crystalline structure and porous morphology of the mesoporous SiO_2 nanoparticles. Figure 1 presents a characteristic TEM micrograph of the nanoparticles, which are mostly identical and sphere-shaped with an average diameter of ~ 100 nm, indicating a high surface area. They also show a highly ordered hexagonal array and streak structural characteristics. The WAXD diffraction pattern of the mesoporous SiO_2 nanoparticles in Fig. 1 shows three diffraction peaks at $2\theta = 2.38°$, 4.12° and 4.76°, which correspond to the (100), (110) and (200) planes of SiO_2, respectively. The repeat distance, a_0, between two pore centers can be obtained from $a_0 = (2/\sqrt{3}) \times d_{100}$ [24]. The pore diameter was determined from a_0 by subtraction of 1.0 nm, which was an estimated value for the thickness of pore wall. Since the calculated

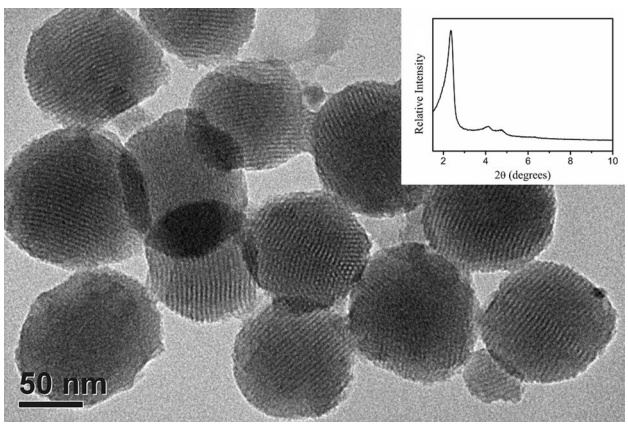

Fig. 1 TEM images of mesoporous SiO_2 nanoparticles. Inserted wide-angle X-ray diffraction of mesoporous SiO_2 nanoparticles

d_{100} value is 3.71 nm, the pore diameter of mesoporous SiO_2 nanoparticles is 3.28 nm. Figure 2a corresponds to a typical TEM micrograph of mesoporous C#SiO_2 nanoparticles. The hexagonal array is no longer observed. The average diameter of these nanoparticles is ~ 120 nm, approximately 20 nm larger than that of the SiO_2 nanoparticles. This indicates that the surface of the nanoparticles is coated with a thin carbon layer. Figure 2b shows the Raman spectra of both mesoporous SiO_2 and C#SiO_2 nanoparticles. The absorption peaks of the former at 480 and 920 cm^{-1} correspond to the surface phonon mode of silica [28]. For the latter, two additional absorption peaks were observed at 1350 and 1580 cm^{-1}, which are assigned to the D and G modes of graphene [29]. This indicates that the surface of carbon coating has a graphene structure.

The chemical structure and morphology of the polypyrrole (PPy)/C#SiO_2 nanocomposites were also characterized by WAXD and FTIR. Figure 3 shows the FTIR spectrum of the nanocomposites. For comparison, the spectra of pure PPy and C#SiO_2 nanoparticles are also presented. In the spectrum of pure PPy, the absorption peaks at 1035 and 900 cm^{-1} correspond to the C–H deformation and C–H out-of-plane vibration, respectively [30]. The peaks at 1550, 1450, and 1175 cm^{-1} can be attributed to the C–N and C–C in-ring stretching modes, and C–N stretching vibration. The absorption peak at 780 and 670 cm^{-1} correspond to the C–H out-of-plane bending and C–C out-of-plane ring deformation vibration, respectively [31]. For the C#SiO_2 nanoparticles, the peak at 1725 cm^{-1} was assigned to the C=O stretching vibration; revealing that the C#SiO_2 nanoparticles contain oxidized functional groups. The spectrum of the PPy/C#SiO_2 nanocomposites was approximately identical to that of PPy, indicating that the surface of the mesoporous C#SiO_2 nanoparticles was coated with PPy. Additionally, the WAXD patterns of the C#SiO_2 nanoparticles, PPy and PPy/C#SiO_2 nanocomposites are presented in Fig. 4. A strong diffraction peak at $2\theta = 2.38°$ corresponds to the (100) plane of the SiO_2 nanoparticles. Moreover, no new diffraction peaks were found in the XRD profile of the PPy/C#SiO_2 nanocomposite; suggesting that the PPy coating has an amorphous structure.

3.2 Electrochemical characterization

The electrochemical performance of the PPy/C#SiO_2 nanocomposites electrodes was evaluated by cyclic voltammetry (CV) curves in a three-electrode test system. The CV curves of bare GCE, PPy and PPy/C#SiO_2 nanocomposite electrodes in 0.1 mM DA at pH 7.0 are presented in Fig. 5. The signal of DA on the bare GCE electrode is weak, and the ΔE between the anodic and cathodic peak is 0.22 V. In contrast, when using the electrode modified with

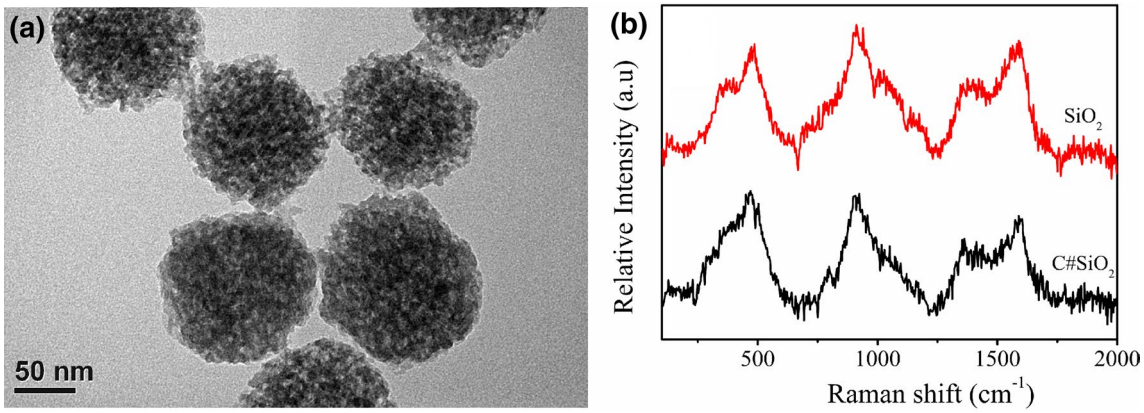

Fig. 2 **a** TEM images of mesoporous C#SiO_2 nanoparticles, **b** Raman spectra of mesoporous SiO_2 and C#SiO_2 nanoparticles

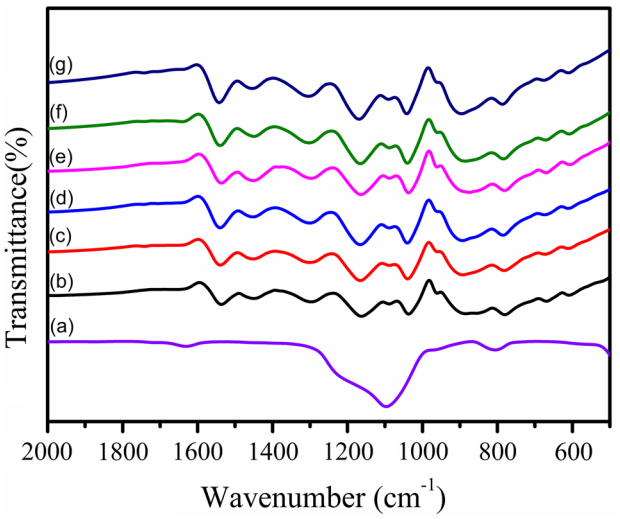

Fig. 3 FTIR spectra of (a) mesoporous C#SiO_2 nanoparticles, (b) neat PPy polymer matrix, (c) 1 wt% PPy/C#SiO_2, (d) 3 wt% PPy/C#SiO_2, (e) 5 wt% PPy/C#SiO_2, (f) 7 wt% PPy/C#SiO_2 and (g) 9 wt% PPy/C#SiO_2 nanocomposites

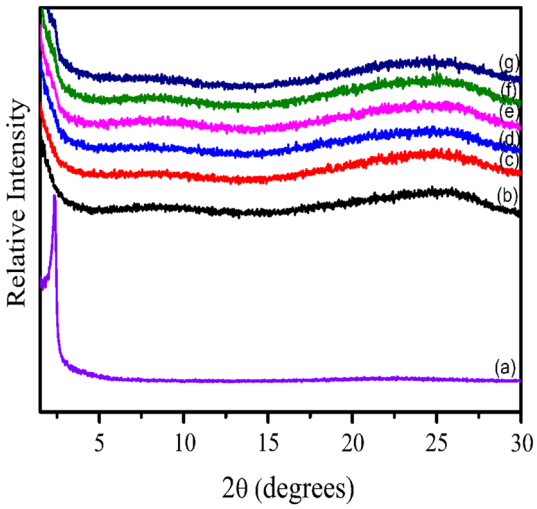

Fig. 4 WAXD diffraction patterns of (a) (a) mesoporous C#SiO_2 nanoparticles, (b) neat PPy polymer matrix, (c) 1 wt% PPy/C#SiO_2, (d) 3 wt% PPy/C#SiO_2, (e) 5 wt% PPy/C#SiO_2, (f) 7 wt% PPy/C#SiO_2 and (g) 9 wt% PPy/C#SiO_2 nanocomposites

conductive PPy (PPy/GCE), the quasi-reversible peak of the DA redox reaction was intense, and the ΔE decreases to 0.12 V. This demonstrates the superior electrochemical performance of the PPy/GCE electrode for DA detection [32]. The oxidation peaks and the peak current when using the PPy/C#SiO_2 nanocomposite electrodes are similar to or larger than those of PPy. This suggests that the PPy-coated mesoporous C#SiO_2 nanoparticles have a higher electrochemical performance than that of PPy. It is likely that the larger surface area induced by the mesoporous C#SiO_2 nanoparticles has an important influence on this result. The highest peak current was obtained with the addition of 5 wt% C#SiO_2 nanoparticles. Increasing their content may lead to aggregation, which would decrease the surface area of the nanocomposites. Therefore, the optimal 5 wt% loading was used for the following measurements.

Electrochemical impedance spectroscopy (EIS) was performed to investigate the interfacial electron transfer properties, such as charge-transfer resistance (R_{ct}) and ion diffusion rate, of the PPy/C#SiO_2 nanocomposites. As seen in Fig. 6, typical Nyquist plots were obtained for bare GCE, PPy and PPy/C#SiO_2 nanocomposite electrodes. All well-defined semicircles, where the diameter (R_{ct}) corresponds to the performance of electrochemical reaction. Low R_{ct} values represent a small charge-transfer resistance at the electrode–electrolyte interface, which should improve the electrochemical performance [33]. For the bare GCE, the R_{ct} value was 1249 Ω. The value

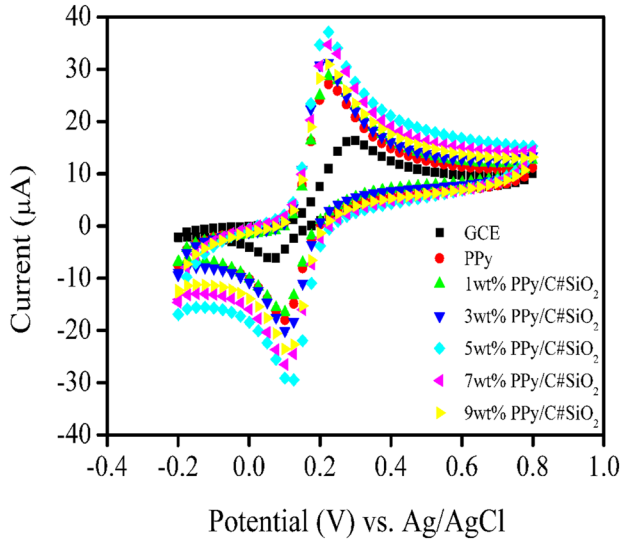

Fig. 5 CV profiles of bare GCE, PPy, various weight ratios of PPy/C#SiO_2 nanocomposites

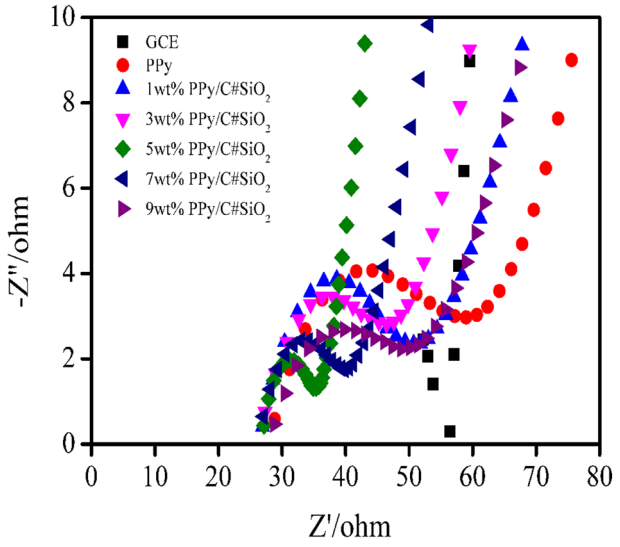

Fig. 6 EIS profiles of bare GCE, PPy, various weight ratios of PPy/C#SiO_2 nanocomposites

greatly decreased for PPy/GCE to 31.0 Ω, indicating that the addition of PPy would significantly reduce the interfacial resistance. When the surface of GCE electrode was modified with 1 wt% PPy/C#SiO_2 nanocomposites (PPy/C#SiO_2/GCE), the R_{ct} value decreased to 24.8 Ω, implying the further improvement of electrochemical performance by the PPy/C#SiO_2 nanocomposite. When the addition of mesoporous C#SiO_2 nanoparticles increased to 3 and 5 wt%, the R_{ct} value decreased to 20.1 and 9.2 Ω. Increasing the content of C#SiO_2 nanoparticles to 7 and 9 wt% led to an increase in the R_{ct} to 13.1 and 21.4 Ω. Therefore, 5 wt% PPy/C#SiO_2 nanocomposite was selected for the following experiments.

Differential pulse voltammetry (DPV) in the potential range of − 0.1 to 0.4 V was carried out to detect DA varying concentrations of DA using the 5 wt% PPy/C#SiO_2/GCE electrode. According to previous report, the determination of DA using polypyrrole-coated palladium silver nanospherical composites showed superior electrocatalyic properties at pH = 7 [34]. Figure 7 shows the dependence of DA oxidation peak current on the concentration of DA at pH = 7. The current increases linearly with the DA concentration in the 1.0×10^{-6} to 2.0×10^{-4} M range. The regression equation obtained was $I(\mu A) = 0.0758\ C_{DA}\ (\mu M) + 0.232$ ($R^2 = 0.996$). The detection limit is approximately 7.6×10^{-7} M based on a signal-to-noise of 3. Table 1 presents a comparison with previous reports on DA detection. It can be seen that the results of this work, including the linear range and detection limit, are similar to those obtained from various modified electrode surfaces.

Since the oxidation potential of DA at bare GCE is very similar to that of AA and UA, it is very difficult to distinguish between compounds due to signals overlapping [35]. Figure 8 displays the DPVs with 5 wt% PPy/C#SiO_2/GCE during consecutive additions of 1.0×10^{-3} M AA, 2.5×10^{-4} M UA and different DA concentrations. The oxidation potentials of AA, DA and UA are − 0.017, 0.113 and

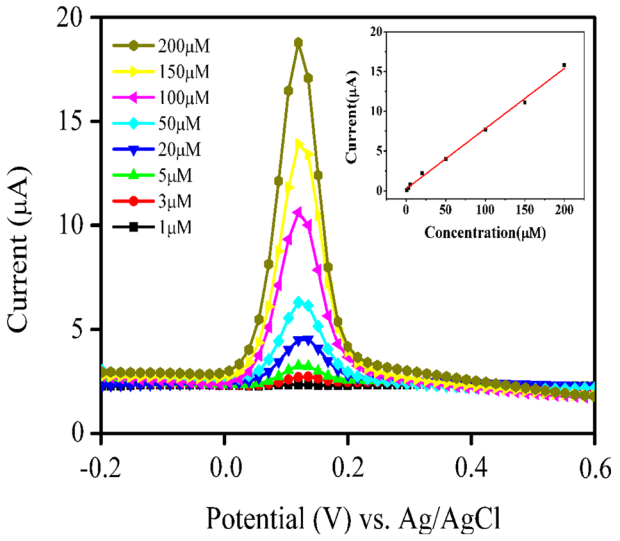

Fig. 7 The profiles of differential pulse voltammetry for 5 wt% PPy/C#SiO_2 nanocomposite electrode containing different concentrations of DA at pH = 7. Inset: Plots of the anodic peak current as a function of DA concentration

Table 1 The detection limits and linear ranges of different modified electrodes for the determination of DA

Electrode	Analytical technique	Linear range (μM)	Detection limit (μM)	Refs.
PPy/Pt/GCE	DPV	1–77	0.6	[36]
PPy/Ag/GCE	DPV	0.5–155	0.1	[37]
PANI-NF/Pt/GCE	DPV	2–10	33.3	[38]
PPy-IC/GCE	CV	10–300	0.1	[39]
PPy/Graphene/GCE	Amperometric	100–1000	2.3	[40]
GO/Fe_3O_4@SiO_2/SCE	DPV	0.1–600	0.09	[41]
Fe3O4/SnO2/Gr/CPE	DPV	20–2800	0.007	[42]
PPy/C#SiO_2/GCE	DPV	1–200	0.7	This work

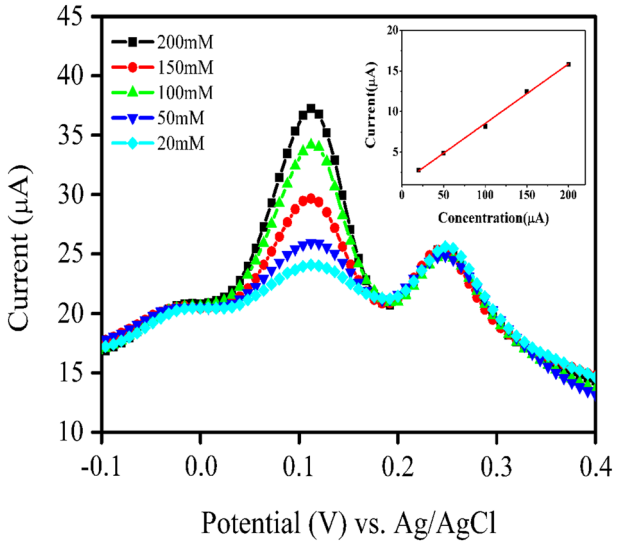

Fig. 8 The profiles of differential pulse voltammetry for 5 wt% PPy/C#SiO_2 nanocomposite electrode containing 1.0×10^{-3} M AA, 2.5×10^{-4} M UA, and different concentrations of DA at pH = 7. Inset: Plots of the anodic peak current as a function of DA concentration

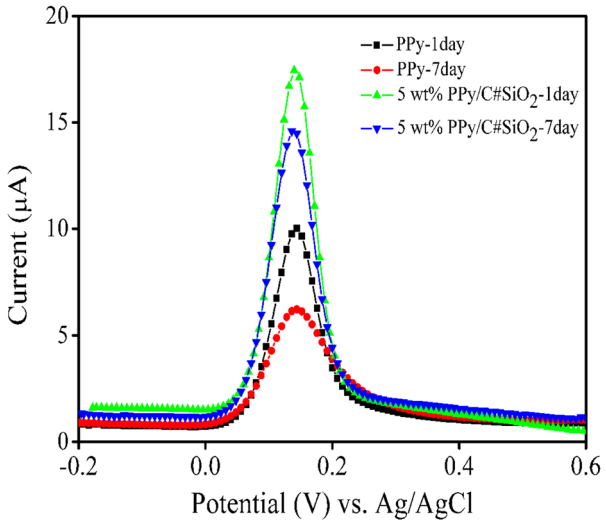

Fig. 9 The profiles of differential pulse voltammetry for PPy and 5 wt% PPy/C#SiO_2 nanocomposite electrode after 1 and 7 days incubation with 200 μM DA

0.248 V. When using the 5 wt% PPy/C#SiO_2/GCE, the separation between peaks is sufficient to avoid the interference of AA and UA for DA detection. This demonstrates that 5 wt% PPy/C#SiO_2/GCE has an exceptional performance for DA determination with an acceptable linear range and detection limit in the presence of AA and UA. To evaluate the stability of the conductive composites, DPV tests were carried out for PPy/GCE and 5 wt% PPy/C#SiO_2/GCE stored for 1 and 7 days. Figure 9 shows the oxidation peak currents of PPy/GCE decreased from 9.1 μA for 1 day of storage to 5.5 μA for 7 day of storage. The tendency was similar for 5 wt% PPy/C#SiO_2/GCE, but the remaining current is significantly higher than that of PPy/GCE. This indicates that the presence of mesoporous C#SiO_2 nanoparticles stabilizes the surface structure of the electrode during long storage periods.

4 Conclusions

In this study, we used core–shell mesoporous C#SiO_2 nanoparticles to prepare a high-performance PPy/C#SiO_2 nanocomposite via in situ chemical-oxidative polymerization. The CV and EIS measurements show that the 5 wt% PPy/C#SiO_2 nanocomposite has high peak current and low charge-transfer resistance, indicating 5 wt% is the optimal nanoparticles loading. A linear response was observed for dopamine detection in the concentration range of 1×10^{-6} to $\times10^{-4}$ M with a detection limit of 7.6×10^{-7} M ($S/N = 3$) for the 5 wt% PPy/C#SiO_2 nanocomposites. These nanocomposites also demonstrate exceptional DA detection in the presence of AA and UA. Because of their excellent electrochemical performance, the PPy/C#SiO_2 nanocomposites may be considered as adequate materials for DA detection.

Acknowledgements Financial support of this work was provided by the Ministry of Science and Technology (MOST) under Grand MOST 107-2212-E-005-020 and the Ministry of Education under the project of Innovation and Development Center of Sustainable Agriculture (IDCSA).

References

1. Luczak T (2008) Electrochemical oxidation of dopamine in the presence of secondary amine. An alternative way for quantitative dopamine determination at a gold electrode. Electroanalysis 20:1639–1646
2. Robinson DL, Hermans A, Seipel AT, Wightman RM (2008) Monitoring rapid chemical communication in the brain. Chem Rev 108:2554–2584
3. Cooper JR, Bloom FE, Roth RH (1982) The biochemical basis of neuropharmacology. Oxford University Press, Oxford
4. Abbaspour A, Khajehzadeh A, Ghaffarinejad A (2009) A simple and cost-effective method as an appropriate alternative for visible spectrophotometry: development of a dopamine biosensor. Analyst 134:1692–1698
5. Carrera V, Sabater E, Vilanova E, Sogorb MA (2007) A simple and rapid HPLC-MS method for the simultaneous determination of epinephrine, nonepinephrine, dopamine, and 5-hydroxytryptamine: application to the secretion of bovine chromaffin cell cultures. J Chromatogr B 847:88–94
6. Canbay E, Akyilmaz E (2014) Design of a multiwalled carbon nanotube–Nafion–cysteamine modified tyrosinase biosensor and its adaptation of dopamine determination. Anal Biochem 444:8–15
7. Zhang W, Yuan R, Chai YQ, Zhang Y, Chen SH (2012) A simple strategy based on lanthanum–multiwalled carbon nanotube nanocomposites for simultaneous determination of ascorbic acid, dopamine, uric acid and nitrite. Sens Actuators B 166:601–607
8. Sheng ZH, Zheng XQ, Xu JY, Bao WJ, Wang FB, Xia XH (2012) Electrochemical sensor based on nitrogen doped graphene: simultaneous determination of ascorbic acid, dopamine and uric acid. Biosens Bioelectron 34:125–131
9. Hsu WF, Wu TM (2019) Electrochemical sensor based on conductive polyaniline coated hollow tin oxide nanoparticles and nitrogen doped graphene quantum dots for sensitively detecting dopamine. J Mater Sci 30:8449–8456
10. Raj CR, Okajima T, Ohsaka T (2003) Gold nanoparticle arrays for the voltammetric sensing of dopamine. J Electroanal Chem 543:127–133
11. Zhang F, Li Y, Gu Y, Wang Z, Wang C (2011) One-pot solvothermal synthesis of a Cu_2O/graphene nanocomposite and its application in an electrochemical sensor for dopamine. Microchim Acta 173:103–109
12. Deng H, Lin L, Ji M, Zhang S, Yang M, Fu Q (2014) Progress on the morphological control of conductive network in conductive polymer composites and the use as electroactive multifunctional materials. Prog Polym Sci 39:627–655
13. Oueiny C, Berlioz S, Perrin FX (2014) Carbon nanotube–polyaniline composites. Prog Polym Sci 39:707–748
14. Omastova M, Trchova M, Kovarova J, Stejskal J (2003) Synthesis and structural study of polypyrroles prepared in the presence of surfactants. Synth Met 138:447–455
15. Hsu FH, Wu TM (2016) Polypyrrole/molybdenum trioxide/graphene nanoribbon ternary nanocomposite with enhanced capacitive performance as an electrode for supercapacitor. J Solid State Electrochem 20:691–698
16. Lin YW, Wu TM (2011) Synthesis and characterization of water-soluble polypyrrole/multi-walled carbon nanotube composites. Polym Int 60:382–388
17. Ghanbari Kh, Babaei Z (2016) Fabrication and characterization of non-enzymatic glucose sensor based on ternary NiO/CuO/polyaniline nanocomposite. Anal Biochem 498:37–46
18. Ji X, Hampsey JE, Hu Q, He J, Yang Z, Lu Y (2003) Mesoporous silica-reinforced polymer nanocomposites. Chem Mater 15:3656–3662
19. Wu W, Zhang S, Zhou J, Xiao X, Ren F, Jiang C (2011) Controlled synthesis of monodisperse sub-100 nm hollow SnO_2 nanospheres: a template- and surfactant-free solution-phase route, the growth mechanism, optical properties, and application as a photocatalyst. Chem Eur J 17:9708–9719
20. Min K, Yoo YJ (2009) Amperometric detection of dopamine based on tyrosinase-SWNTs-PPy composite electrode. Talanta 80:1007–1011
21. Zhou X, Ma P, Wang A, Yu C, Qian T, Wu S, Shen J (2015) Dopamine fluorescent sensors based on polypyrrole/graphene quantum dots core/shell hybrids. Biosens Bioelectron 64:404–410
22. Ghanbari KH, Bonyadi S (2018) An electrochemical sensor based on reduced graphene oxide decorated with polypyrrole nanofibers and zinc oxide–copper oxide p–n junction heterostructures for the simultaneous voltammetric determination of ascorbic acid, dopamine, paracetamol, and tryptophan. New J Chem 42:8512–8523
23. Wei A, Pan L, Huang W (2011) Recent progress in the ZnO nanostructure-based sensors. Mater Sci Eng B 176:1409–1421
24. Cai Q, Luo ZS, Pang WQ, Fan YW, Chen XH, Cui FZ (2001) Dilute solution routes to various controllable morphologies of MCM-41 silica with a basic medium. Chem Mater 13:258–263
25. Mikhailenko S, Desplantier-Giscard D, Danumah C, Kaliaguine S (2002) Solid electrolyte properties of sulfonic acid functionalized mesostructured porous silica. Microporous Mesoporous Mater 52:29–37
26. Vinu A, Hossain KZ, Ariga K (2005) Recent advances in functionalization of mesoporous silica. J Nanosci Nanotech 5:347–371
27. Shehab M, Ebrahim S, Soliman M (2017) Graphene quantum dots prepared from glucose as optical sensor for glucose. J Lumin 184:110–116
28. Glinka YD, Jaroniec M (1997) Spontaneous and stimulated Raman scattering from surface phonon modes in aggregated SiO_2 nanoparticles. J Phys Chem B 101:8832–8835
29. Wu TM, Lin YW, Liao CS (2005) Preparation and characterization of polyaniline/multi-walled carbon nanotube composites. Carbon 43:734–740
30. Lu XJ, Zhang F, Dou H, Yuan CZ, Yang SD, Hao L, Shen LF, Zhang LJ, Zhang XG (2012) Preparation and electrochemical capacitance of hierarchical graphene/polypyrrole/carbon nanotube ternary composites. Electrochim Acta 69:160–166
31. Aguilar-Hernandez J, Potje-Kamloth K (1999) Optical and electrical characterization of a conducting polypyrrole composite prepared by in situ electropolymerization. Phys Chem Chem Phys 1:1735–1742
32. Li Y, Jiang Y, Mo T, Zhou H, Li Y, Li S (2016) Highly selective dopamine sensor based on graphene quantum dots self-assembled monolayers modified electrode. J Electroanal Chem 767:84–90
33. Wang J, Li Y, Ge J, Zhang BP, Wan W (2015) Improving photocatalytic performance of ZnO via synergistic effects of Ag nanoparticles and graphene quantum dots. Phys Chem Chem Phys 17:18645–18652
34. Mahmoudian MR, Basirun WJ, Alias YB (2016) A sensitive dopamine biosensor based on polypyrrole coated palladium silver nanospherical composites. Ind Eng Chem Res 55:6943–6951
35. Liu L, Li S, Liu L, Deng D, Xia N (2012) Simple, sensitive and selective detection of dopamine using

dithiobis(succinimidylpropionate)-modified gold nanoparticles as colorimetric probes. Analyst 137:3794–3799
36. Mazzotta E, Caroli A, Primiceri E, Monteduro AG, Maruccio G, Malitesta C (2017) All-electrochemical approach for the assembly of platinum nanoparticles/polypyrrole nanowire composite with electrocatalytic effect on dopamine oxidation. J Solid State Electrochem 21:3495–3504
37. Ghanbari K, Hajheidari N (2015) Simultaneous electrochemical determination of dopamine, uric acid and ascorbic acid using silver nanoparticles deposited on polypyrrole nanofibers. J Polym Res 22:152
38. Bagherzadeh M, Mozaffari SA, Momeni M (2015) Fabrication and electrochemical characterization of dopamine-sensing electrode based on modified graphene nanosheets. Anal Methods 7:9317–9323
39. Rui Z, Huang W, Chen Y, Zhang K, Cao Y, Tu J (2017) Facile synthesis of graphene/polypyrrole 3D composite for a high-sensitivity non-enzymatic dopamine detection. J Appl Polym Sci 134:44840
40. Lee CY, Hsu DY, Prasannan A, Kalaivani R, Hong PD (2016) Facile synthesis of hexagonal-shaped polypyrrole self-assembled assembled particles for the electrochemical detection of dopamine. Appl Surf Sci 363:451–458
41. Beitollahi H, Nejad FG, Shakeri S (2017) GO/Fe_3O_4@SiO_2 core–shell nanocomposite modified graphite screen-printed electrode for sensitive and selective electrochemical sensing of dopamine and uric acid. Anal Methods 9:5541–5549
42. Bagheri H, Pajooheshpour N, Jamali B, Amidi S, Hajian A, Khoshsafar H (2017) A novel electrochemical platform for sensitive and simultaneous determination of dopamine, uric acid and ascorbic acid based on Fe_3O_4-SnO_2-Gr ternary nanocomposite. Microchem J 131:120–129